Liquid CO2 behaviour during water displacement in a sandstone core sample

Liquid CO_2 Behaviour during Water Displacement in a Sandstone Core Sample

Ebraheam Al-Zaidi*, Xianfeng Fan

Institute for Materials and Processes, School of Engineering, The University of Edinburgh, King's Buildings, Mayfield Road, Edinburgh, EH9 3JL, United Kingdom

* Corresponding author. Tel.: +44-782-407-776 or +964-771-715-5652. E-mail address: e.al-zaidi@ed.ac.uk or ebraheam80_saheb@yahoo.com.

Abstract: CO_2 sequestration in saline aquifers and hydrocarbon reservoirs is a potential strategy to reduce CO_2 concentration in the atmosphere, enhance hydrocarbon production, or extract geothermal heat. CO_2 injection is considerably influenced by the interfacial interactions, capillary forces and viscous forces. Any change in the subsurface conditions of pressure, temperature, and salinity is likely to have an impact on the interfacial interactions, capillary forces and viscous forces, which, in turn, will have an influence on the injection, migration, displacement, and CO_2 storage capacity. In this study, unsteady-state immiscible experimental investigations have been performed to explore the impact of fluid pressure, temperature, salinity (brine concentration and valency) and injection rate on the dynamic pressure evolution and displacement efficiency when CO_2 as a liquid phase is injected into a water-saturated sandstone core sample. This study also highlights the impact of capillary forces and viscous forces on the two-phase flow properties and shows when capillary forces or viscous forces are dominant. The results reveal a moderate to considerable impact for the fluid pressure, temperature, injection rate, and salinity on the differential pressure profile, water recovery (*WR*), endpoint CO_2 relative permeability ($KrCO_2$), and cumulative produced volumes. Overall, increasing fluid pressure, CO_2 injection rate and salinity (brine concentration and valency) cause an increase in the differential pressure profile; the highest increase occurred with the injection rate. In general, increasing temperature caused a reduction in the differential pressure profile. The *WR* is in range of around 61.6-69.3% while the $KrCO_2$ is in range of 0.112-0.203, depending on the investigated parameters. Increasing fluid pressure and injection rate caused an increase in the *WR*; the highest increase occurred with the injection rate. On the other hand, increasing temperature and salinity caused a decrease in the *WR*; the highest reduction occurred with salinity. Nevertheless, the increase in fluid pressure, temperature, injection rate and salinity led to a reduction in the endpoint CO_2 relative permeability; the highest reduction occurred with increasing temperature whilst the lowest occurred with increasing fluid pressure. The cumulative injected volumes decreased with fluid pressure and salinity but showed no noticeable change with temperature and injection rate. The capillary forces have less impact on the differential pressure profiles than viscous forces when fluid pressure, temperature and injection rate increase but the capillary forces have more impact when salinity increase.

1 Introduction

Carbon capture and storage CCS is regarded as one of the promising techniques to reduce CO_2 concentration into the atmosphere [1-3], enhance hydrocarbon recovery, or extract geothermal heat from subsurface formations [4, 5]. The captured CO_2 can be injected into deep saline aquifers, depleted or abandoned oil and gas reservoirs [5-7], unmineable coal bed seams [5, 8], and deep oceanic waters (depths > 3000 m) [9]. As a result, the injected CO_2 can exist in a supercritical state ($ScCO_2$) (e.g., Weyburn oil field:~140 bar, 49.85 °C), a gaseous state (GCO_2) (e.g., Alabama Black Warrior Basin:~70 bar, 22.85 °C), and/ or a liquid state (LCO_2) (e.g., West Sak reservoir: ~110-125 bar, 23.9 °C [10, 11] and deep oceanic waters [9]), as shown in Figure 1, [10-15]. Liquid CO_2 can also be used as a working fluid to enhance oil recovery in high-temperature reservoirs [16]. Hamdi and Awang showed a significant enhancement in the displacement efficiency when a low-temperature CO_2 (liquid CO_2) is injected into a hot reservoir (+ 93 °C)[16].

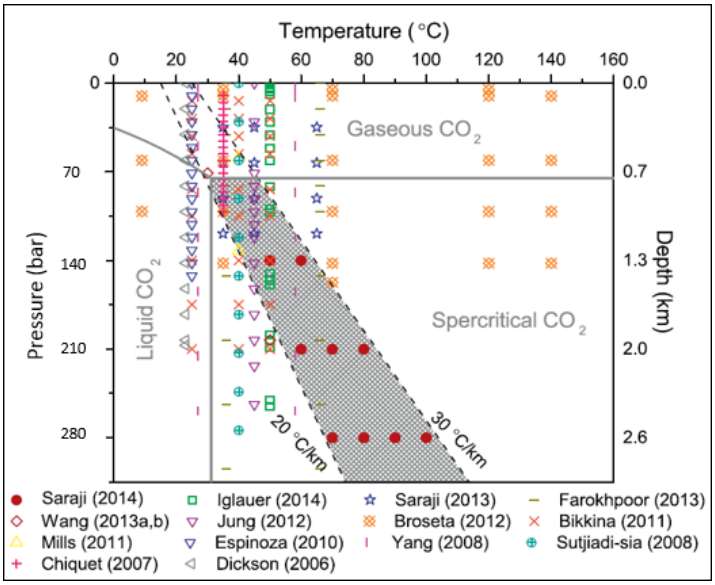

Figure 1: The pressure and temperature ranges at which saline aquifers are found underground [14].

During CO_2 injection in subsurface formations, although some bulk CO_2 will be eventually dissolved in formation water with time, at early stages most of the injected CO_2 will displace the formation water in an immiscible displacement [17, 18]. The displacement of the injected CO_2 depends the interfacial interactions (e.g. interfacial tension, wettability, capillarity, and mass transfer across the interface [19, 20]) between the injected CO_2, formation water, and formation rock in host formation as well as the injection rate and its duration, the densities and viscosities of the injected and present fluids, petrophysical properties of the host formation [21, 22], viscous forces and capillary forces.

Characterization of the multiphase flow of immiscible displacements under various conditions is of significant interest for many industrial and environmental issues such CO_2 injection, fluid migration, storage capacity and long-term fate of CO_2 storage in saline aquifers [23-25], CO_2-enhanced oil and gas recovery processes [7, 26]. Any change in subsurface conditions of pressure, temperature, and salinity (e.g. salt's type (NaCl, $CaCl_2$, $MgCl_2$ [27, 28]), valency and concentration) will have an impact on the interfacial interactions [8, 12, 27, 29-31], the viscous forces [32] and the capillary forces, which, in turn, influence the multiphase flow characteristics by affecting relative permeability, capillary pressure-saturation relationship [33, 34], relative permeability [34], pore-scale fluid distribution [35], and residual trapping [33]. In reality, a change in temperature is expected to occur as liquid CO_2 moves downward injection wells. Liquid CO_2 injection to displace oil form layers with different depths is also anticipated to be accompanied by a temperature change.

The role of brine salinity is attributed to its ability to change CO_2 solubility, interfacial tension between fluids [36, 37], wettability of caprock and aquifers [28, 31, 38, 39], and effective permeability [40]. Thereby, changing salinity is likely to have an impact on oil recovery [38, 41-45], and the capacity and security of CO_2 storage in underground formations [14, 46, 47]. Researchers have shown that changing salt type and valency resulted in a different impact on wettability, permeability and storage capacity [27, 28, 48]. Xu et al. showed that using NaCl and $CaCl_2$ brines lead to a different wettability behaviour as NaCl monovalent brine has a highly water-wet tendency while $CaCl_2$ divalent brine has an oil-wet tendency [48]. Wu and Firoozabadi noticed that NaCl, KCl, and $CaCl_2$ have an adverse and a different impact on permeability; increasing NaCl salinity led to a reduction in gas absolute permeability; while, increasing $CaCl_2$ salinity caused only a minor impact on permeability [28]. Arif et al. noticed an increase in zeta potential and a concomitant increase in contact angle; i.e. shifting wettability towards oil-wet, when divalent cations (Mg^{2+}, and Ca^{2+}) was used. They observed that using brine instead of deionised water caused a reduction in the storage capacity, which was attributed to surface de-wetting, and that the storage capacity with NaCl was higher than that of $MgCl_2$ and $CaCl_2$ due to better wetting performance [27]. Thus, although salinity is one of the key parameters that strongly influence the CO_2–brine displacements in both microscopic and macroscopic flows, it has not attracted much attention in previous investigations [31, 49]. Moreover, most of studies provided in literature have focused on investigating salinity impact on the properties of CO_2-water (brine) systems (e.g. wettability and interfacial tension) with scarce or overlooked attention to salinity impact on multiphase flow properties of CO_2-water (brine) systems.

The characterization of multiphase flow of CO_2-water (brine) system involves laboratory experiments [50], computational modelling [50-52], and field scale projects [24]. The current literature review showed an extensive work has been done to investigate supercritical CO_2-brine (water) displacements [18, 21, 49, 53-65] but only a scarce research

has been allocated to gaseous [66-68] and liquid CO_2 (LCO_2)-water displacements [22, 25, 54, 60, 69]. Song et al. examined the multiphase properties of LCO_2-water displacements, under immiscible conditions of 60 bar and 21.85 °C, in a packed bed filled with glass beads. They noticed that: (**I**) in general, the efficiency of water displacement depends on the permeability, displacement pattern, and CO_2 injection rate, (**II**) low permeability formations leads to an increase in the residual water saturation, and (**III**) CO_2 fingering or channelling phenomena occur even in liquid immiscible displacement [54]. Levine et al. examined flow-properties of LCO_2-water/brine (1%, and 5% NaCl)-displacements, in synthetic and natural porous media (Berea sandstone core sample) at 100 bar and 20 °C, by measuring the differential pressure against various flowrates. They noticed that drainage endpoint relative permeability of LCO_2 was between 0.34 and 0.44 [25]. Zhang et al. investigated the impact of pore-scale heterogeneity on the two-phase characteristics of CO_2-water displacement by conducting LCO_2-water displacements inside a dual permeability pore network model at 90 bar and 22 ± 1 °C. They noticed that at low injection rate, the displacement is unstable, and the water is displaced by LCO_2 from high permeability zones only. However, as CO_2 injection rate increased, the displacement mechanism shifted from capillary to viscous fingering, and liquid CO_2 displaced water from lower permeability zones, too [22]. Alemu et al. injected LCO_2 into a brine-saturated Rothbach sandstone core sample at 100 bar and 20 °C. After 20 pore volumes (PVs) of CO_2 injection, the endpoint residual CO_2 saturation was 0.53 [60]. Manceau et al. injected LCO_2 into a water-saturated Triassic sandstone core sample at 90 bar and 28 °C; the Triassic core sample contains small amounts of carbonate minerals. As a result of the CO_2 injection, they observed a mineral dissolution and an increase in porosity and permeability [69]. It can be seen that aforementioned LCO_2-water displacements have investigated different topics such as: (**a**) the two-phase flow properties in different porous media, (**b**) pore-scale heterogeneity impact on two-phase flow characteristics, (**c**) endpoint residual CO_2 saturation, (**d**) mineral dissolution, and (**e**) porosity and permeability change. Nevertheless, despite its high importance, these studies have overlooked the analysis of the pressure data in core flooding [70].

In our previous study [71], we have investigated the impact of CO_2 phase on the pressure and production data. In this investigation, we have explored the impact of the fluid pressure, temperature, salinity, and injection rate on the dynamic pressure evolution and displacement efficiency when a CO_2 in its liquid state is injected into a water/brine (1% NaCl, 1% $CaCl_2$, and 5% NaCl) saturated sandstone core sample under unsteady-state immiscible conditions. This study also highlights the impact of capillary forces and viscous forces on the two-phase flow properties and shows when the capillary forces or viscous forces are dominant. This study deals with the impact of the investigated parameters on the two-phase flow characteristics, especially focusing on the differential pressure profile, water production profile, residual water saturation, and effective and relative CO_2 permeabilities. During these dynamic displacements, the transient pressures were recorded at the inlet and outlet sides of the core; and, the differential pressure, transient out flowrates of water and CO_2, water recovery, and endpoint effective (relative) CO_2 permeability were measured and analysed. To the authors' best knowledge, no detailed experimental investigation have been presented in literature yet. The result of this study would be of an interest for the injection, displacement, migration, and storage capacity and integrity of CO_2 in deep and cold formations. It is worth mentioning that in our previous study [71], we explored the impact of injection rate on the differential pressure of LCO_2-water displacements. In this study, detailed investigations focus on the injection rate impact on the differential pressure as a function of fluid pressure.

2 Materials and Experimental Setup

A sandstone core sample from Guillemot A Field in the North Sea saturated with dionised water was used during these unsteady-state immiscible liquid CO_2-water drainage displacements. The core sample has a diameter of 2.54 cm, length of 7.62 cm, an average effective porosity of 14%, and an absolute water permeability of 15.8 millidarcy; for more information about the core sample description see Al-Zaidi et al [71].

2.1 Experimental Setup

As shown in Figure 2, the experimental system used for performing liquid CO_2–drainage displacements are consisted of two high-pressure syringe pumps (Teledyne ISCO, Lincoln, NE, United States, flow range of 0.0001 to 30 ml/min with an accuracy of 0.3% of set point), a stainless steel core holder, a pressure gauge mounted on the core holder for measuring confining pressure, a water bath (Grant instruments GD 100) for controlling the temperature with a precision of ± 0.02 ˚C, an overburden pressure pump (CM400) for delivering the confining pressure, a vacuum pump (Edwards, Model E2M5) for removing the trapped gas, pressure transducers (UNIK, 0-100 bar with a precision of ± 0.1% of BSL) for measuring the pressure readings at the inlet and outlet side of the core; and a LabVIEW software system built for acquiring the pressure readings from the pressure transducers.

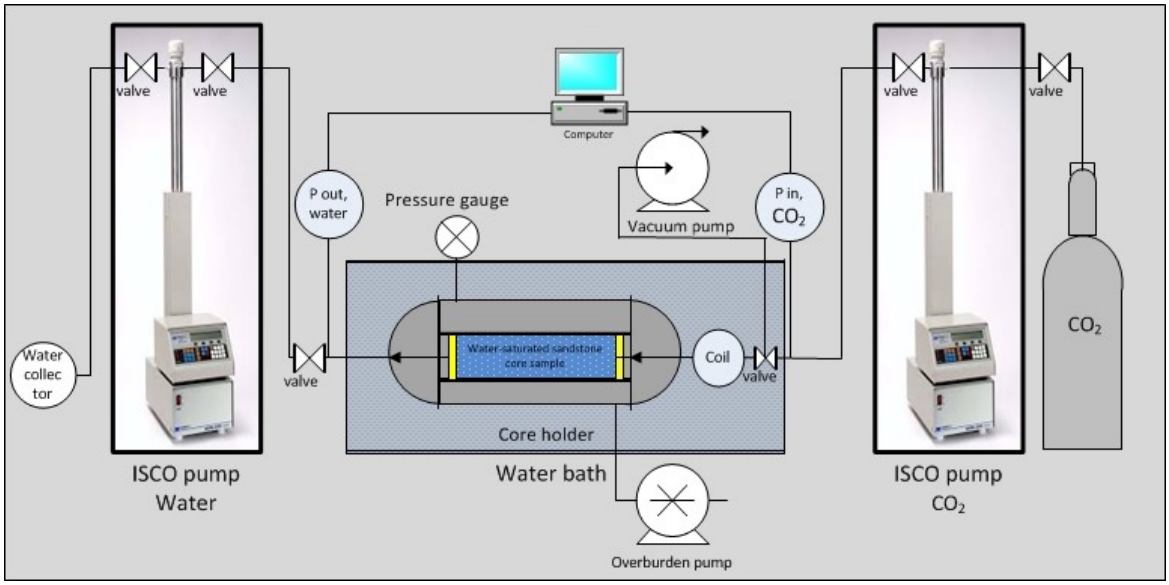

Figure 2: The experimental setup for Liquid CO_2-water displacements.

2.2 *Liquid CO_2-Water Drainage Displacement procedures*

First of all, the core sample was wrapped into a shrinkable Teflon tube and placed inside a rubber sleeve. Then, the core sample was placed inside the core holder, which was mounted horizontally inside the water bath. Next, the overburden pump was run to deliver a confining pressure of about 135 bar, which was always higher than the pore pressure, for avoiding fluid bypassing the core sample. Later, the water bath was filled with water, temperature was controlled by the heater, and vacuum pump was connected to the system to remove the trapped gas. To fully saturate the core sample with water, about 40-60 pore volumes (PVs) of deionised water was injected at a high-differential pressure of 80-90 bar; this differential pressure was attained by using a 0.2 μm membrane (Nuclepore Track-Etch Membrane-Whatman). To obtain heat equilibrium, the water bath temperature was set to the required degree and the system was left overnight at the experimental temperature.

Prior to each flooding experiment, a constant pressure was applied to the entire system with the syringe pump at each end. After achieving the experimental pressure, the system was left for about 20 mins to ensure that temperature stabilization is achieved throughout the system. Later, the mode of the injection pump was changed from a constant pressure mode to a constant flowrate mode, and the CO_2 was injected (at a constant injection rate) into the water saturated core sample. The volumes of the injected CO_2 and collected fluids were recorded every 30 seconds. During the experiment, the inlet and outlet pressure transducer readings were recorded every 6 seconds, using the LabVIEW software, in order to calculate the differential pressure across the core sample. When the experiment was finished, the volumes produced were measured to calculate the residual water saturation using the mass balance principles. Later, the weight of the core sample was measured using a Sartorius weighing scale with a resolution of 0.0001 gram to confirm the residual saturation measurements.

3 Results and Discussions

In order to have a deep insight into the two-phase flow characteristics when a liquid CO_2 is injected into sandstone formations, the effect of fluid pressure, temperature, injection rate and salinity (brine concentration and valency) on the differential pressure profile, production behaviour, water recovery, and endpoint effective and relative permeabilities of CO_2 have been investigated. The experimental data has been categorized into three main sections. The first and second main sections deal with the impact of fluid pressure, temperature, injection rate and salinity on the differential pressure profile and production behaviour, respectively; while the third section deal with their influence on the endpoint CO_2 effective (relative) permeability and residual water saturation. It should be noted that during this study, the corresponding time refers to the time required to reach the maximum-differential pressure at the start of the experiment. The quasi-differential pressure refers to the differential pressure at the end of the core flooding.

The differential pressure of LCO_2-water displacements can be obtained by having the difference between the pressure transducers readings at the inlet and outlet sides of the core sample. In a horizontal flooding process, the differential pressure is largely influenced by the capillary and viscous forces. The capillary forces are dependent on the

CO_2-water interfacial tension, contact angle, pore diameter and geometry [34, 74-76] while the viscous forces are controlled by the viscosity of both displacing and displaced fluids, fluid velocity in the pores, the amount of each fluid (i.e. the length of CO_2 invasion) in the pore, and the properties of the porous medium (e.g. cross sectional area, permeability and length). The capillary forces arise when an interface exists between the immiscible fluids [74]. The capillary forces are highly influenced the multiphase flow in low permeability rocks and fractured reservoirs [77] and responsible for the entrapment of one phase by another in a porous medium during immiscible flooding processes [75, 78]. Espinoza and Santamarina [12] propose the following equation to account for the differential pressure when a liquid CO_2 displaces brine (water) in a cylindrical horizontal tube:

$$\Delta P = P_{CO2} - P_{water} = 4\,\frac{\sigma_{CO_2-water}\,COS\theta}{d} + v\,\frac{32\,L}{d^2}\left(\frac{l_{CO_2}\mu_{CO_2}+l_{water}\mu_{water}}{L}\right) \quad (1)$$

where ΔP is the differential pressure across the core sample (Pa). P_{CO2} and P_{water} are the CO_2 phase and water bulk pressures, respectively. $\sigma_{CO2\text{-}water}$ is the CO_2-water interfacial tension (mN/m), θ the contact angle between fluids and core sample surface, d (m) the diameter of the largest effective pore [79-82], v (m/sec) the fluid velocity in the pores, L (m) the length of the core sample, l (m) length of CO_2 or water phase inside the core sample, and μ (Pa·s) the viscosity of the fluids. Eq.1 consists of Young-Laplace equation, the first hand-right term, for capillary forces and Poiseuille's equation, the second hand-right term, for viscous forces [12, 83]. In case of small injection rate and high viscosity contrast conditions [83], Eq.1 can be reduced to the Yong-Laplace equation, Eq.2, as follows:

$$\Delta P = P_{CO2} - P_{water} = 4\,\frac{\sigma_{CO_2-water}\,COS\theta}{d} \quad (2)$$

3.1 Differential Pressure Profile of Liquid CO_2-Water Drainage Displacements

To examine the effect of fluid pressure, experimental temperature, salinity (brine concentration and valency), and CO_2 injection rate on the differential pressure and production behaviour, series of LCO_2-water (brine) displacements were conducted at various fluid pressures (from 60 to 90 bar), different experimental temperatures (20 and 29 °C) and various CO_2 injection rates (0.1, 0.4 and 1ml/min).

3.1.1 Effect of Fluid Pressure on the Differential Pressure Profile of Liquid CO_2-Water Displacements

The data from Figure 3 and Figure 4 present the impact of increasing fluid pressure on the differential pressure profile. It is worth mentioning that the differential pressure for the 60 bar-displacements in Figure 3 and Figure 4 were presented in our previous paper [71]; however, they have been used here to make a comparison with the 70 bar-displacements. The differential pressure profile experienced a sharp increase that is followed by a quasi-stable pressure reduction for a while; and then, it experienced a high-pressure reduction that is followed by a gradual pressure reduction. Increasing fluid pressure led to an increase in the differential pressure profile, which further increased with increasing injection rate. For illustration, as the fluid pressure increased from 60 to 70 bar, the differential pressure during the early times of the flooding increased by around 11% (from around 0.45 to 0.5 bar) for the displacements conducted at 0.4 ml/min and by around 14% (from around 1.58 to 1.8 bar) for the displacements performed at 1 ml/min; however, the differential pressure at the end of the displacements increased by around 11% (from 0.222 to 0.247 bar) for the displacements conducted at 0.4 ml/min and by around 17.5% (from 0.706 to 0.829 bar) for the displacements performed at 1 ml/min.

According to Eq.1, the most likely reason behind the increase in the differential pressure profile is the increase in the applied viscous forces. This is because the observed increase in the differential pressure profile is the net result of the increase in the viscous forces and the reduction in the capillary forces. With increasing pressure, the viscous forces are increased due to increasing CO_2 viscosity while the capillary forces are reduced due to decreasing CO_2-water interfacial tension (from around 34.9 to 29.7 mN/m as can be seen in Figure 5), and increasing contact angle (owing to increasing CO_2 solubility with increasing pressure) [32]. To confirm that the increase in the differential pressure profile with increasing fluid pressure was because of increasing viscous forces due to increasing CO_2 viscosity, the data presented in Figure 3 were normalized against CO_2 viscosity. The result was an identical trend between the pressure profile of both 60 and 70 bar-experiments, as shown in Figure 6. This confirms that in the case of liquid CO_2-water displacements, the viscous forces are more influential than capillary forces with increasing fluid pressure.

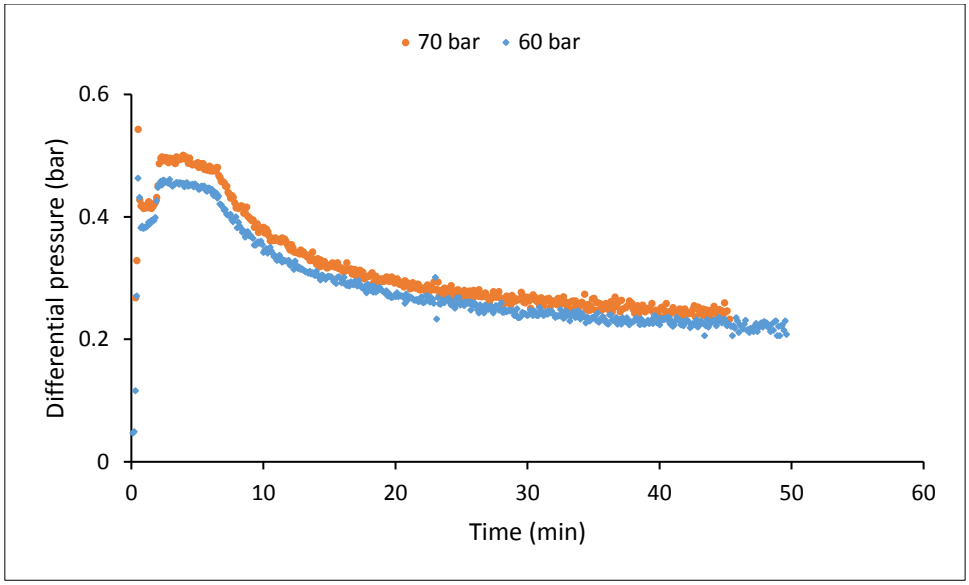

Figure 3: Effect of fluid pressure on the differential pressure profile of LCO_2-water displacements conducted at 0.4 ml/min and 20 °C.

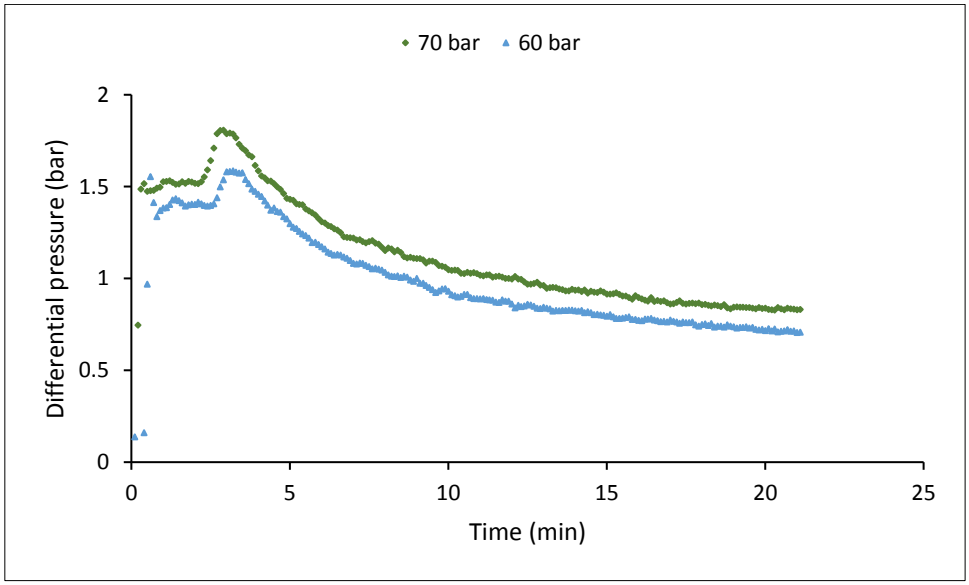

Figure 4: Effect of fluid pressure on the differential pressure profile of LCO_2-water displacements conducted at 1 ml/min and 20 °C.

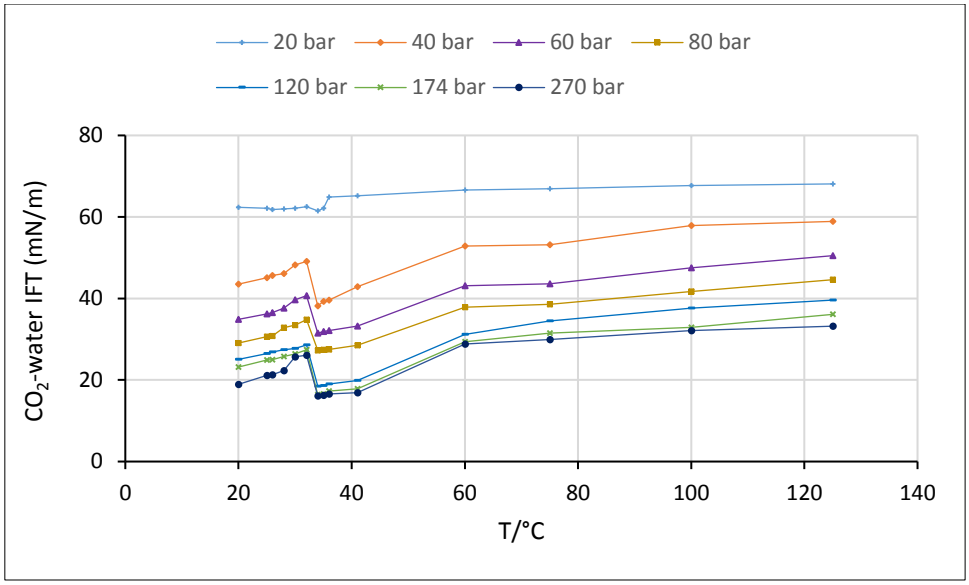

Figure 5: Interfacial tension for CO_2-Pure Water Systems adopted from Bachu and Bennion [32].

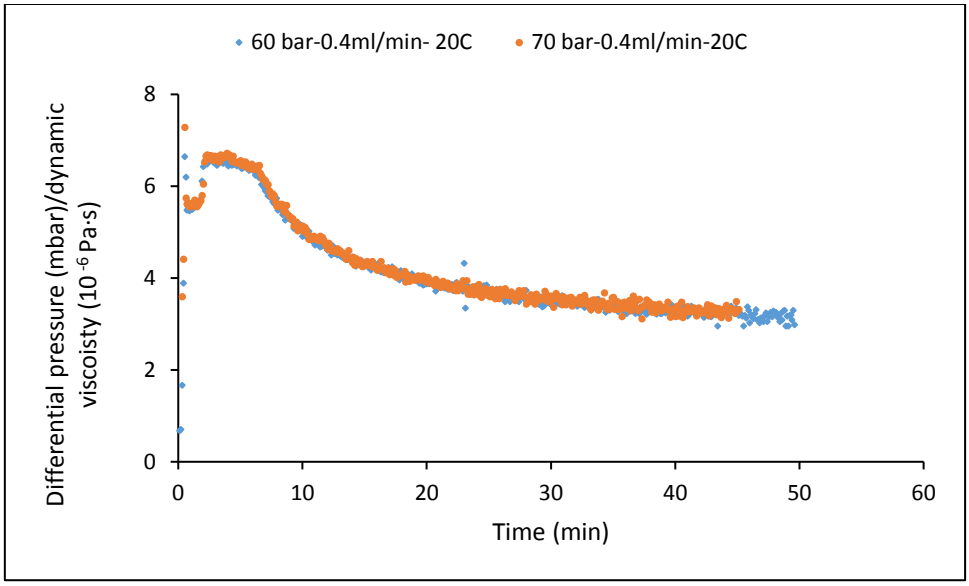

Figure 6: A viscosity normalised differential pressure profiles of LCO_2-water displacements conducted at 20 °C and 0.4 ml/min.

3.1.2 *Effect of Temperature on the Differential Pressure Profile of Liquid CO_2-Water Displacements*

Figure 7 presents the impact of increasing temperature on the differential pressure profile. The results show that the differential pressure profile was stable during the first period that lasted for about 16 min, was reducing overtime during the mixed period, and was increasing over time during the last period; consequently, after around 200 min, the differential pressure profile of the 29 °C-experiment became higher than that of the 20 °C-experiment; the first period, mixed and last period is characterized by water production only, CO_2 and water production, and CO_2 production only, respectively, for more information see Al-Zaidi et al. [71]. Moreover, the results reveal that increasing temperature generated oscillations in the differential pressure profiles. The increase in the differential pressure profile is likely to occur because of the blocking of the CO_2 outflow paths when the viscous forces become less than the capillary forces [84]. The second possible reason is that, after around 170 min, the impact of viscous forces might become higher than that of capillary forces as most of the water was displaced; thereby CO_2 was flowing through opened pores [85]. The oscillations might have occurred as the energy of the CO_2 molecules increased with increasing temperature.

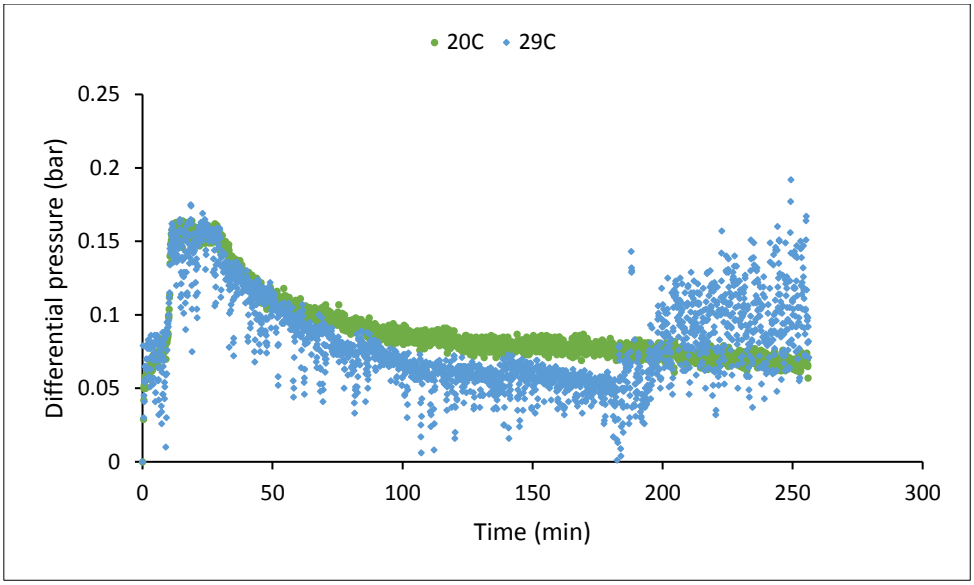

Figure 7: Effect of temperature on the differential pressure profile of LCO_2-water displacements conducted at 90 bar and 0.1 ml/min.

3.1.3 Effect of Injection Rate on the Differential Pressure Profile of Liquid CO_2-Water Displacements

Figure 8 shows the impact of increasing injection rate on the differential pressure profile; while Figure 9 presents the dynamic change in the differential pressure profile with increasing CO_2 injection rate; it is worth stating again that the data in Figure 8 were presented in our previous paper [71], but introduced here for comparison purpose. The increase in injection rate leads to three identifiable observations (**A-C**):

A) The data from Figure 8 show that increasing injection rate resulted in a considerable increase in the differential pressure, which was slightly decreased (by around 3%) with increasing fluid pressure. For illustration, increasing injection rate for the 60 bar-experiments caused the maximum-differential pressure to increase by more than 236% (from 0.463 to 1.554 bar) and the quasi-differential pressure to increase by 240% (from 0.208 to 0.707 bar). Nonetheless, increasing the injection rate for the 70 bar-experiments caused the maximum-differential pressure to increase by around 233% bar (from 0.543 to 1.807 bar) and the quasi-differential pressure to increase by 237% (from 0.247 to 0.832 bar) According to Eq.1, the observed increase in the maximum and quasi-differential pressures can be related only to the increase in viscous forces due to the increase in the CO_2 injection rate. However, the observed reduction in the differential pressures can be associated with the reduction in the capillary forces with increasing fluid pressure as stated in Section 3.1.10 above.

B) The data from Figure 9 show that increasing CO_2 injection rate from 0.4 to 1 ml/min caused the differential pressure to increase by more than 3.5 times, except for the first 5 min interval. During this time interval, the ratio of the differential pressures decreased quickly from around 3.5 to 2.5 times. The quick reduction in the differential pressure might reflect the high replacement of the water (a more viscous fluid) by CO_2 (a less viscous one) and the high increase in the CO_2 relative permeability at the expense of water relative permeability. After 5 min until the end of the experiment, the differential pressure ratio profiles (Figure 9) experienced a quasi-steady profile. This indicates that the majority of water production happened during the first 5 min, therefore the capillary and viscous forces experienced a slight reduction (as most water was produced and most capillaries were opened to flow [85]) leading to a small reduction in the differential pressure profile ratio.

C) The data from Figure 8 reveal that increasing injection rate caused a high spike in the differential pressure profile after the initial increase, which is immediately followed by a sharp reduction that is followed by a gradual reduction. The spikes in the differential pressure immediately before CO_2 breakthrough might have occurred because of the sweeping of water inside the pipeline segments [56] or it might happen because the injected CO_2 had to open new flow

paths after the initial entry as the available space was not enough for the injected CO_2, which depends on the core sample properties.

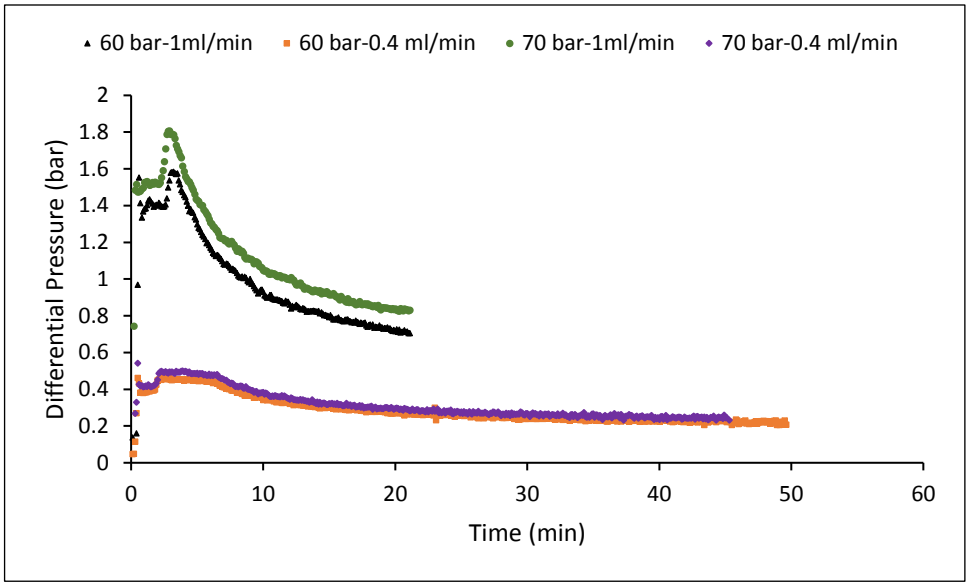

Figure 8: Effect of injection rate on the differential pressure profile of LCO_2-water displacements conducted at 60 bar and 20 °C.

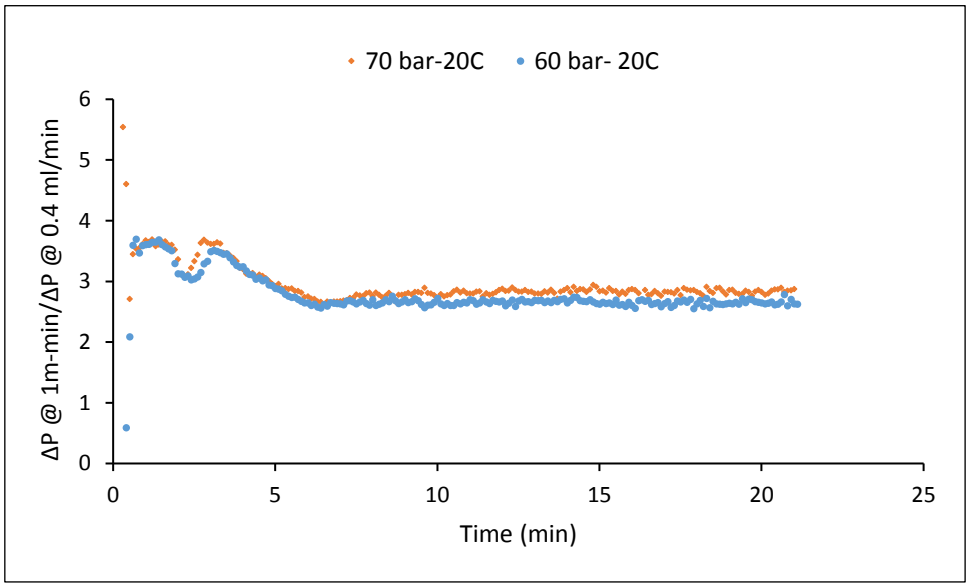

Figure 9: The ratio of the differential pressure of 1 ml/min-experiment to the differential pressure of the 0.4 ml/min-experiment for LCO_2-water displacements conducted at 60 and 70 bar and 20 °C.

3.1.4 *Effect of Salinity on the Differential Pressure Profile OF Liquid CO_2-Brine (Water) Displacements*

Figure 10 and Figure 11 present the impact of brine concentration and valency on the differential pressure profile at different injection rates. The results reveal that increasing brine concentration and valency caused a slight increase in the differential pressure profile with a slight change in the differential pressure profile, mainly during the first period.

Figure 10 shows that increasing brine concentration and valency led to a slight increase in the differential pressure profile, primarily during the first period. Overall, the order of the differential pressure was as follows: LCO_2-1% $CaCl_2$ > LCO_2-5% NaCl > LCO_2-1% NaCl > LCO_2-DIW displacement. According to Eq.1, the increase in the differential pressure can be related largely to the increase in the capillary forces because of increasing surface tension with increasing brine concentration and valency [86]. The order of the differential pressure was according to the cations arrangement in terms of their order of impact on the increase in surface tension: $Cs^+ < Rb^+ < NH^{4+} < K^+ < Na^+ < Li^+ < Ca^{2+}$ Mg^{2+} [86].

Figure 11 reveals that both deionised water and 1% NaCl displacements showed similar differential pressure profiles. On the other hand, both 1% $CaCl_2$ and 5% NaCl–displacements profiles characterized by almost identical profiles; their profiles were characterized by a spike before starting declining. This sharp increase might have needed in order to open new pores for the injected CO_2.

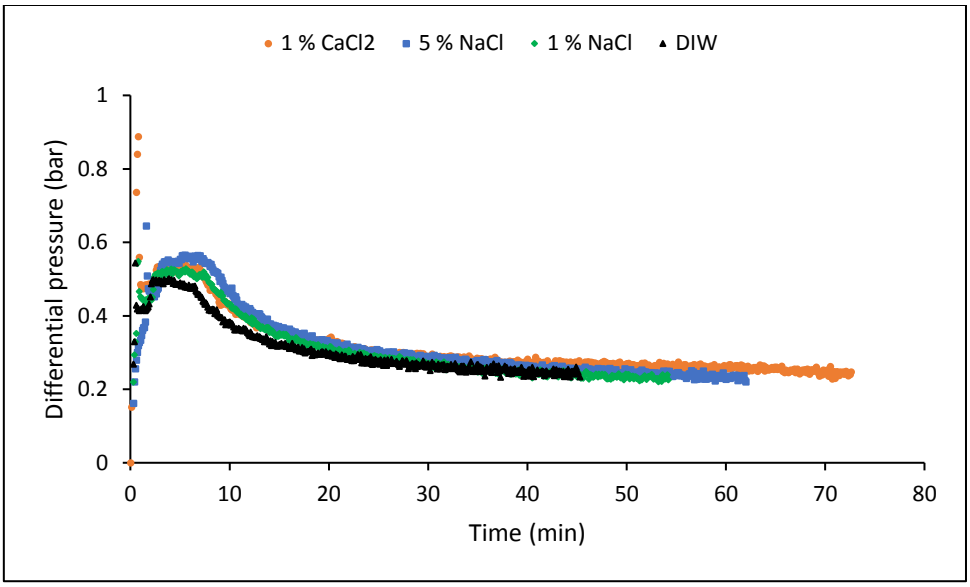

Figure 10: Effect of salinity on the differential pressure profile of LCO_2-brine (DIW) displacements conducted at 70 bar, 0.4 ml/min, and 20 °C.

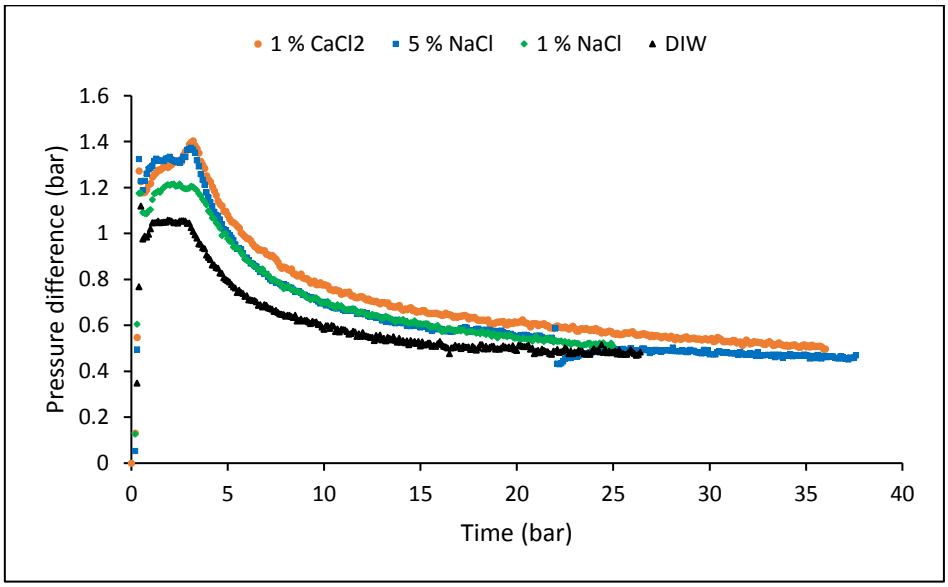

Figure 11: Effect of salinity on the differential pressure profile of LCO_2-brine (water) displacements conducted at 70 bar, 1 ml/min, and 20 °C.

In summary, the differential pressure profile experienced a sharp increase that is followed by a quasi-stable pressure reduction for a while; and then, it experienced a high-pressure reduction that is followed by a gradual pressure reduction. The differential pressure profile characterized by: (**a**) no change in its shape with increasing pressure, (**b**) oscillations and an increase in the differential pressure profile at the end of the displacements with increasing temperature, (**c**) a spike in the differential pressure profile after the initial increase with increasing injection rate, and (**d**) only a slight change, mainly during the first period, with increasing salinity (brine concentration and valency).

The differential pressure profile: (**a**) slightly increased with increasing pressure; which increased with increasing injection rate, (**b**) was stable during the first period, decreased during the mixed period, and increased again during the last period with increasing temperature, (**c**) considerably increased with increasing injection rate, mainly during the first five minutes; this considerable increase was slightly decreased by around 0.3% as the fluid pressure increased from 60 to 70 bar, and (**d**) slightly increased, mainly during the first period, with increasing salinity. The order of the

differential pressure profile with increasing salinity was as follows: LCO_2-1% $CaCl_2$ > LCO_2-5% NaCl > LCO_2-1% NaCl > LCO_2-DIW.

3.2 *Water Production Behaviour*

In this section, we will discuss the effect of fluid pressure, temperature, CO_2 injection rates, and water salinity on the production behaviour.

3.2.1 *Effect of Fluid Pressure on Liquid CO_2-Water Production Behaviour*

Figure 12, Figure 13 and Figure 14 present the transient outflow rates of water and CO_2, the cumulative injected volumes and cumulative produced volumes, and water recovery profile for LCO_2-water displacements, respectively. It is worth mentioning that the differential pressure for the 60 bar-displacements in Figure 14 were presented in our previous paper [71], but included here for comparison with the 70 bar-displacements. The results reveal that increasing fluid pressure led to a slight reduction in the cumulative produced volumes along with the slight increase in water recovery.

The data from Figure 12 and Figure 13 reveal that increasing fluid pressure led to a slight reduction in the transient outflow rates of water and CO_2 and the cumulative produced volumes. As the pressure increased from 60 to 70 bar, the cumulative produced volumes at the end of the experiments decreased slightly by around 0.373 ml. This slight reduction can be related to increasing solubility and compressibility of liquid CO_2 with increasing fluid pressure [87, 88].

The data from Figure 14 show that increasing fluid pressure caused a slight increase in the total water recovery (*WR*) with a very slight increase in the amount of water production and the length of the first period. As the fluid pressure increased from 60 to 70 bar, the *WR* increased by around 2% (from 65.9 to 67.87%) and the water production of the first period increased by 0.003 PVs (from about 0.503 to 0.506 PVs) while its length increased by 0.2 min (from around 6.5 to 6.7 min) due to the slight decrease in the viscosity ratio. The slight increase in the total water production might be related to the increase in the capillary number (*Ca*) and the slight decrease in the viscosity ratio (*M*). The *Ca* increases with the increase in the viscous forces (because of increasing viscosity), and the reduction in the capillary forces (owing to increasing contact angle and reducing CO_2-water interface with increasing CO_2 solubility [12, 80, 83]. As the fluid pressure increased from 60 to 70 bar at a constant temperature of 20 °C, CO_2 viscosity increases from 69.72 to 74.54 × [10^{-6} (Pa·s)], the IFT decreases from 34.9 to 30 mN/m, the *M* decreases from 14.33 to 13.4 and the *Ca* increases from 2.175 to 2.73 × 10^{-7}.

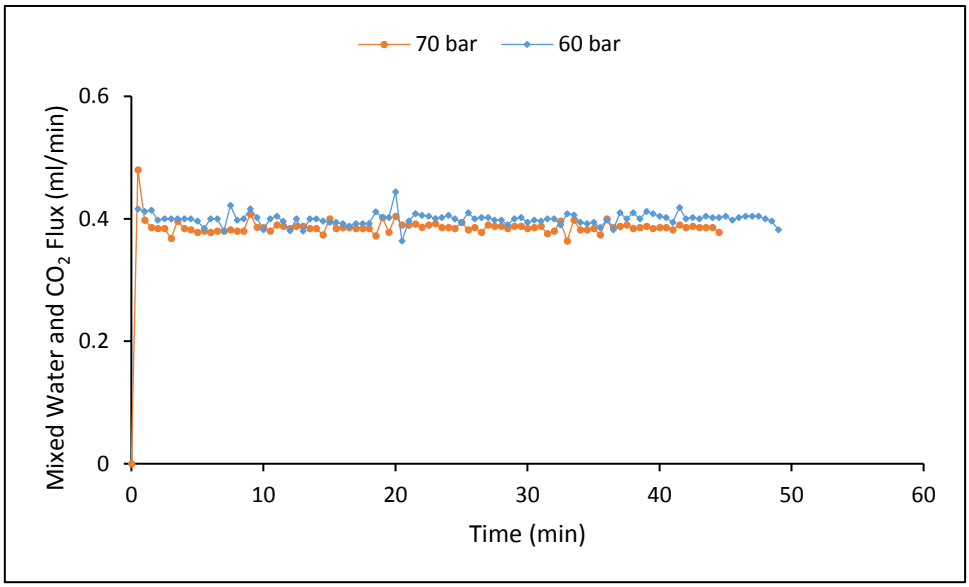

Figure 12: Effect of fluid pressure on the transient outflow rates of water and CO_2 of LCO_2-water displacements conducted at 0.4 ml/min and 20 °C.

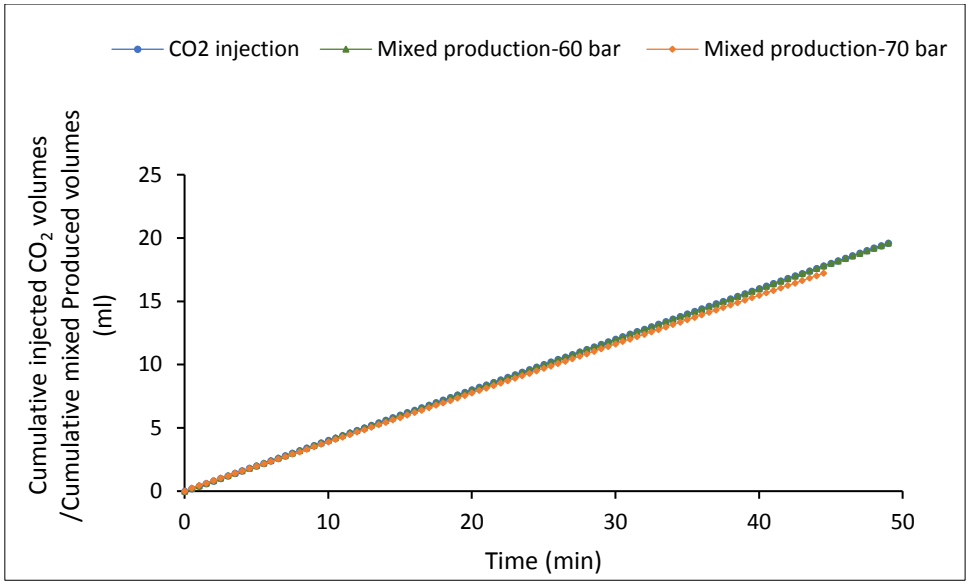

Figure 13: Effect of fluid pressure on the cumulative injected volumes of CO_2 and the cumulative produced volumes of water and CO_2 of LCO_2-water displacements conducted at 0.4ml/min and 20 °C.

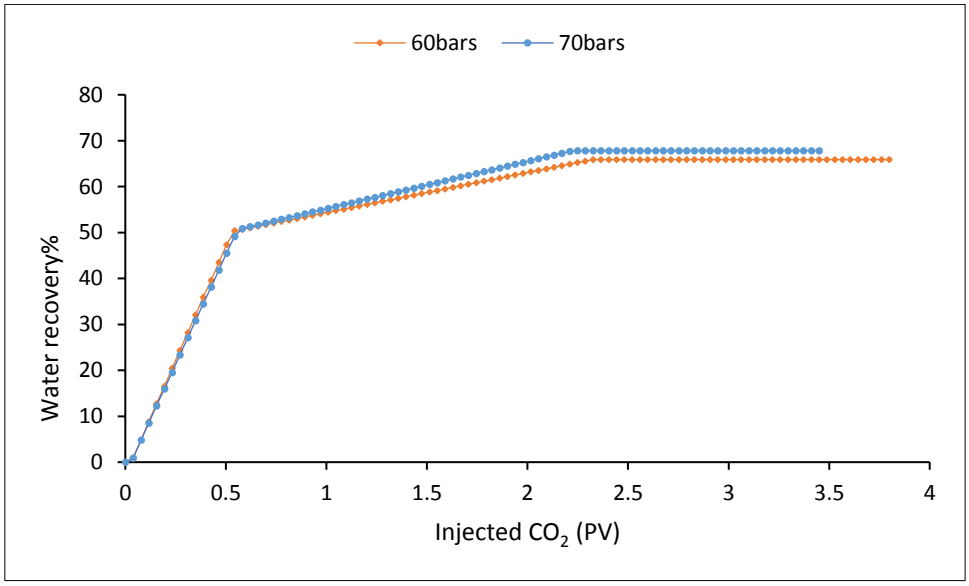

Figure 14: Effect of fluid pressure on the water recovery profile of LCO_2-water displacements conducted at 0.4 ml/min and 20 °C.

3.2.2 *Effect of Temperature on Liquid CO_2-Water Production Behaviour*

Figure 15 presents the effect of increasing temperature on the cumulative injected volumes and the cumulative produced volumes. The data reveals that the cumulative injected volumes of liquid CO_2 were much higher than the cumulative produced volumes. The increase in temperature did not accompanied by a noticeable change in the cumulative volume due to the high-density nature of liquid CO_2 phase, especially at high pressure (90 bar). The difference between the injected and cumulative volumes might be related to the increase in the CO_2 compressibility and the solubility of CO_2 in water, especially at high pressure [12, 80, 83]. It should be noted that the water recovery profile and the transient outflow rate data were not presented here to avoid repeatability as they were similar to those presented in the fluid pressure section above.

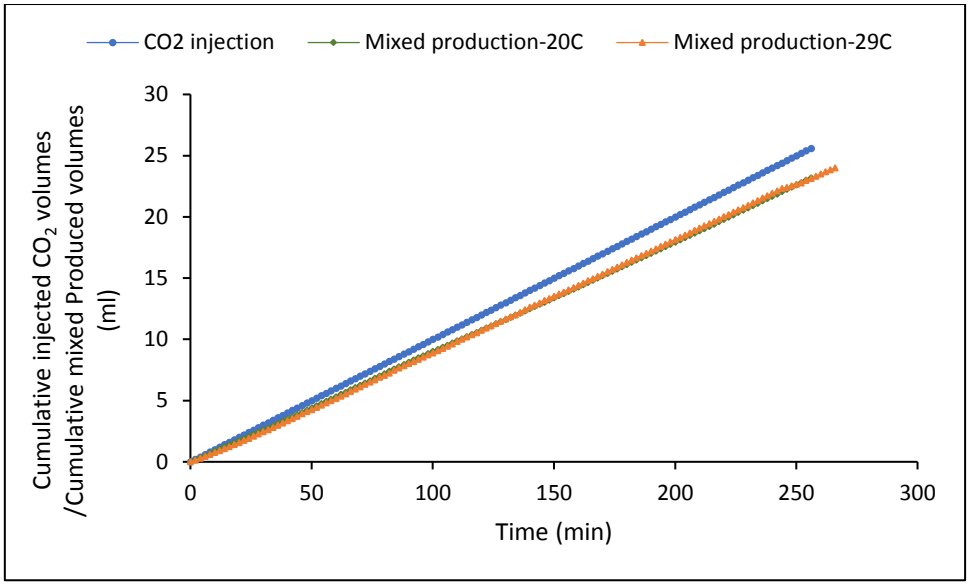

Figure 15: Effect of temperature on the cumulative injected volumes of CO_2 and the cumulative produced volumes of water and CO_2 of LCO_2-water displacements conducted at 90 bar and 0.1 ml/min.

3.2.3 *Effect of Injection Rate on Liquid CO_2-Water Production Behaviour*

The data from Figure 16 to Figure 21 exhibit the impact of increasing CO_2 injection rate on the transient outflow rates, cumulative produced volumes and water recovery profiles at different flowrate. It should be noted that only the data for the LCO_2-water displacement conducted at CO_2 injection rates of 1 ml/min are presented here as the data for 0.4 ml/min was discussed in our previous paper [71] but used here for comparison. The results reveal that the increase in the injection rate caused an increase in the water recovery but caused no observable change in the behaviour of the transient flowrates of water and CO_2 and the cumulative produced volumes.

The data from Figure 16 to Figure 21 reveal that increasing CO_2 injection rate led to: (**I**) a reduction in the time of the only water production period (from around 6.9 to 3.5 min) and that of mixed production period (from about 23 to 6.5 min) , (**II**) a reduction in the amount of water production during only water production period (from 50.37 to 49%) but an increase in that of mixed period (from to 16.3 to 17.38%), and (**III**) an increase in the total water recovery (*WR)* by around 3.4% (from 65.9 to 69.38%) [49] and reduction in the amount of injected CO_2 to achieve that by around 48% (from 2.32 to 1.98 PVs). The increase in the *WR* with increasing injection rate can be associated with the increase in the *Ca* (from about 2.175 to 5.437 × 10^{-7} due to the increase in the viscous forces), and the occurrence of the uniform CO_2 front that leads to increasing CO_2 displacement efficiency [54]. The results suggest that if the goal of CO_2 injection is to enhance displacement efficiency, then a high injection rate might be better.

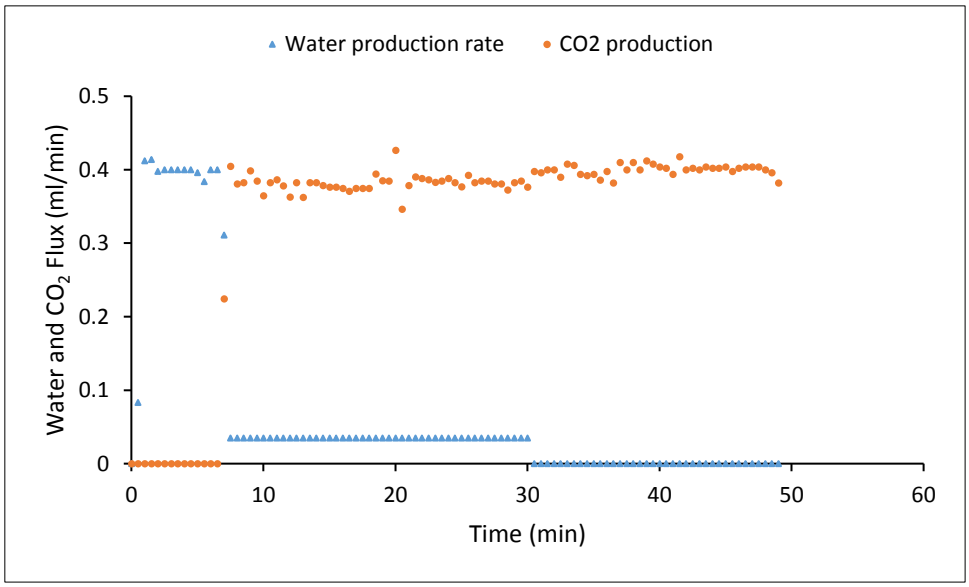

Figure 16: Transient flowrates of water and CO_2 of a LCO_2-water displacement conducted at 60 bar, 0.4 ml/min and 20 °C.

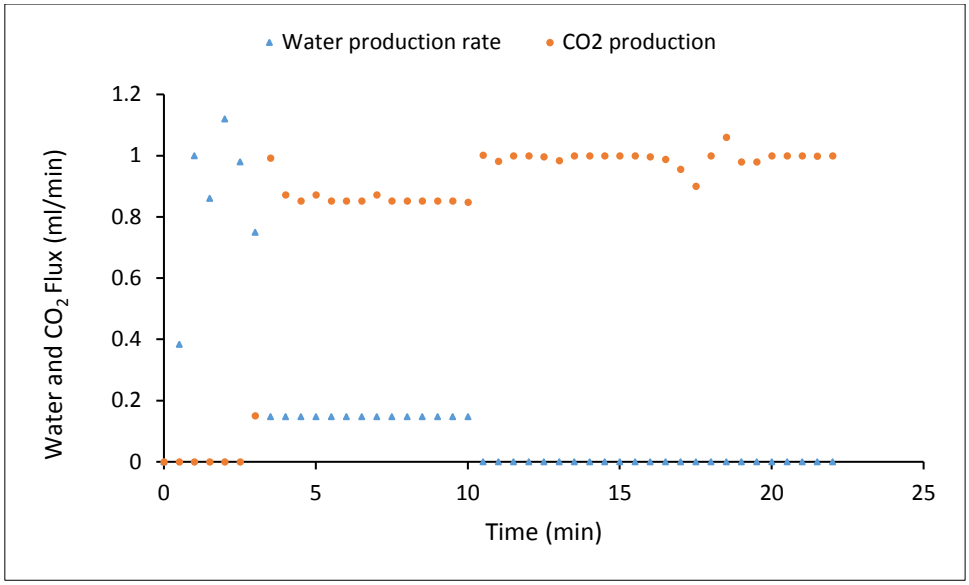

Figure 17: Transient flowrates of water and LCO_2 of a LCO_2-water displacement conducted at 60 bar, 1 ml/min, and 20 °C.

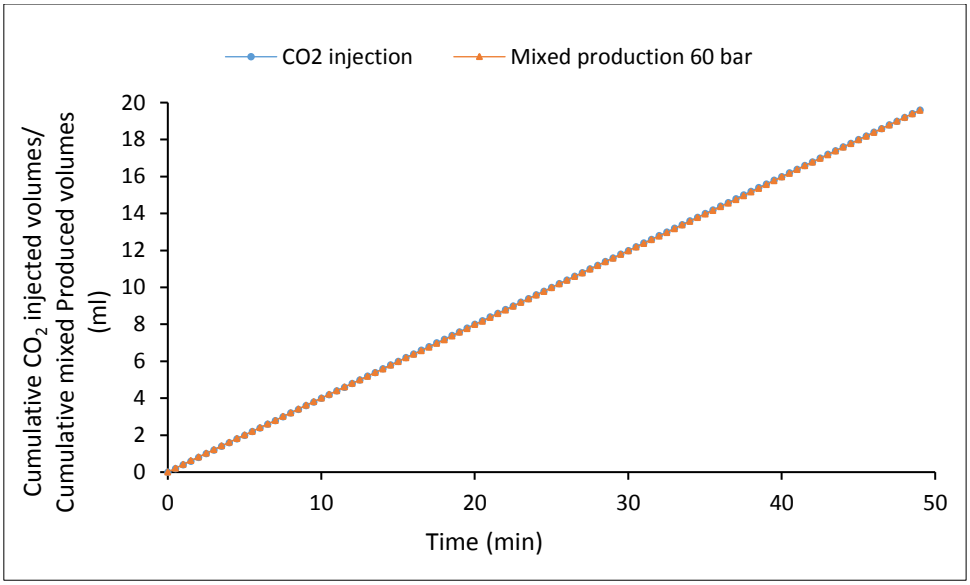

Figure 18: Cumulative injected CO_2 volumes and cumulative produced water and CO_2 volumes for a LCO_2-water displacement conducted at 60 bar, 0.4 ml/min and 20 °C.

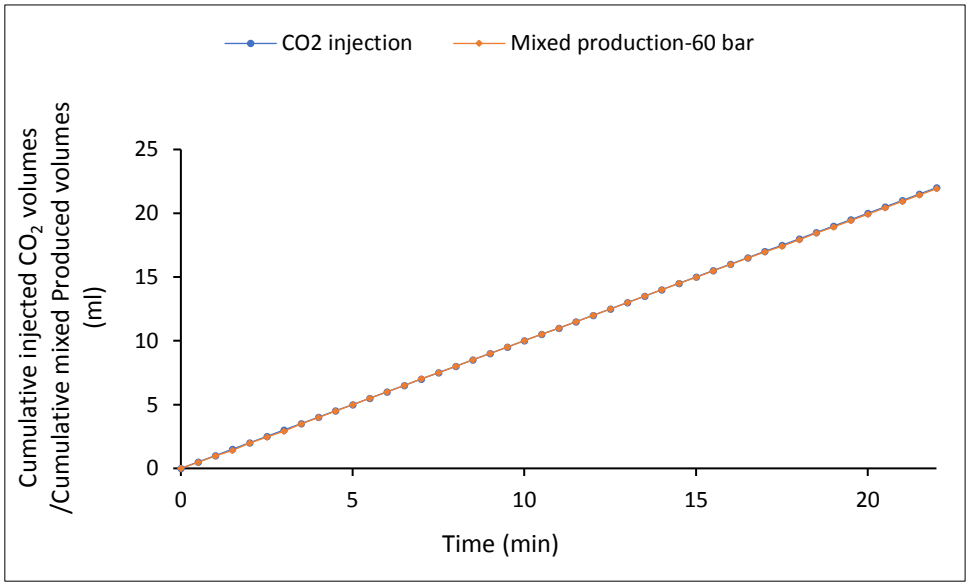

Figure 19: Cumulative injected volumes of CO_2 and cumulative produced volumes of water and CO_2 for LCO_2-water displacement conducted at 60 bar, 1 ml/min, and 20 °C.

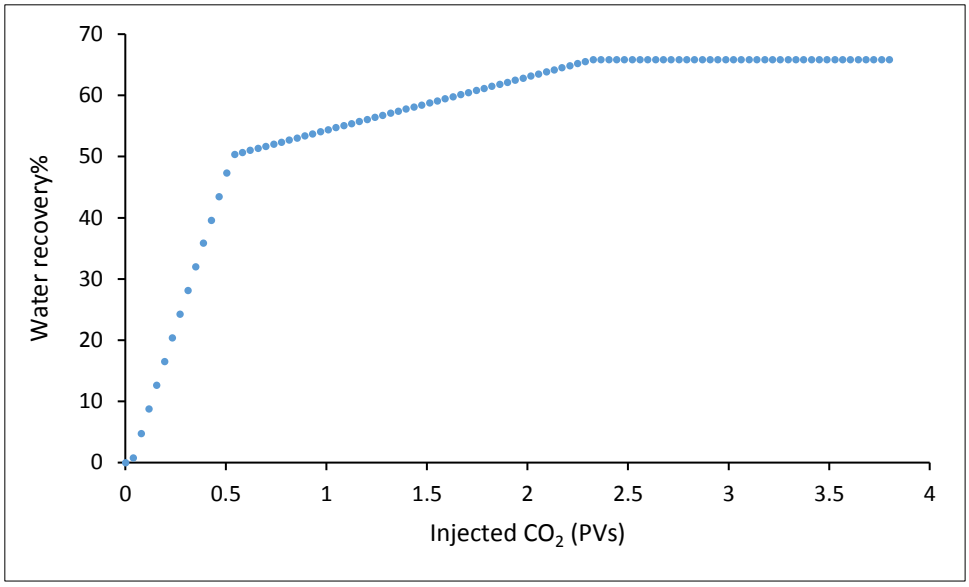

Figure 20: Water recovery of a LCO_2-water displacement conducted at 60 bar, 0.4 ml/min and 20 °C.

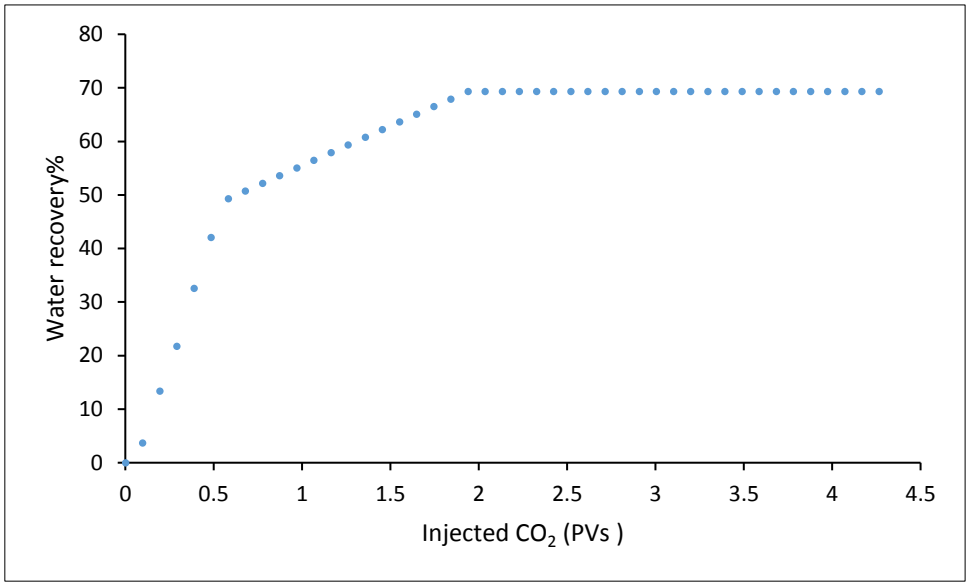

Figure 21: Water recovery of a LCO_2-water displacement conducted at 60 bar, 1 ml/min, and 20 °C.

3.2.4 *Effect of Salinity on Liquid CO_2-Water Production Behaviour*

Figure 22 presents the effect of increasing brine concentration and valency on the cumulative injected volumes and the cumulative produced volumes. The data reveals that the cumulative injected volumes of CO_2 were higher than the cumulative produced volumes. The increase in brine concentration and valency caused a slight decrease in the cumulative produced volumes. The cumulative produced volumes were decreased by around 0.42, 0.62, and 1.07 ml when 1% NaCl, 1% $CaCl_2$, and 5% NaCl was used instead of deionised water, respectively. This might be associated with the reduction in brine recovery due to the increase in capillary forces with the increase in the interfacial tension. However, this reduction cannot be associated with CO_2 solubility as solubility decreases with increasing salinity [89, 90], therefore should increase the produced CO_2 volumes.

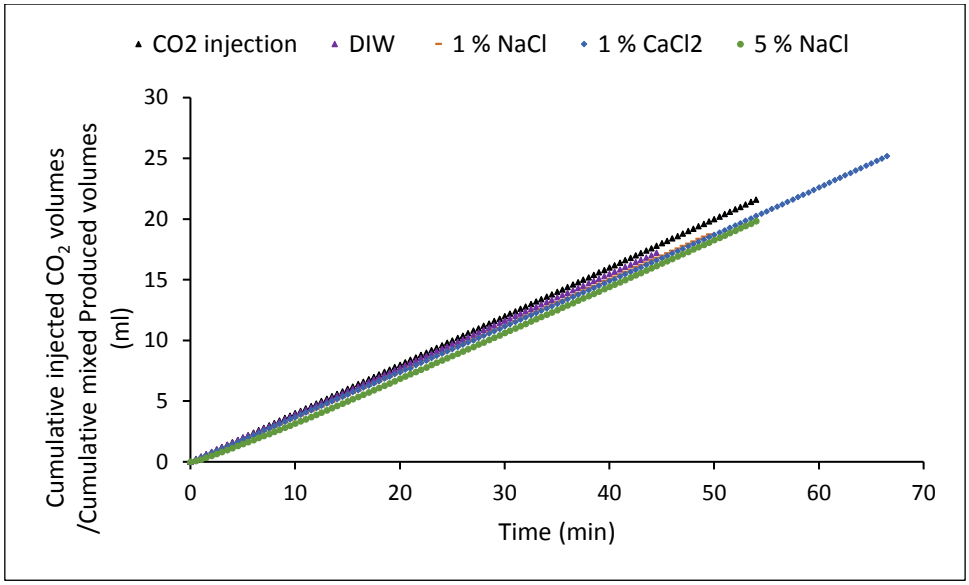

Figure 22: Effect of salinity on the cumulative injected volumes of CO_2 and the cumulative produced volumes of water and CO_2 volumes for LCO_2-water displacements conducted at 70 bar, 0.4 ml/min, and 20 °C.

In summary, the cumulative produced volumes: (a) decreased slightly with increasing fluid pressure and salinity, and (b) showed no noticeable change with increasing temperature and injection rate. The *WR* increased with increasing pressure and injection rate. The amounts of injected LCO_2 volumes to achieve the highest *WR* were reduced as injection rate increased.

3.3 Effect of Fluid Pressure, Temperature, Injection Rate, and Salinity and Valency on Endpoint Effective (Relative) Permeability and Water (Brine) Recovery

The effective and relative permeabilities of CO_2 are of practical interest for determining the efficiency and integrity of CO_2 sequestration in subsurface formations [40, 91]. At the end of the flooding experiment, the volume of the produced water was measured, and the residual water saturation was calculated. Then, the core sample was weighed to confirm the calculated residual water saturation. To calculate the endpoint effective (K_{fCO2}) permeability and endpoint relative permeability (K_{rCO2}) of liquid CO_2 using Darcy's law, the average differential pressure and the average CO_2 outflow rate of the last period were used [56, 92]. The CO_2 viscosity at the fluid pressure and experimental temperature was calculated using the Peace software website [93]. It should be noted that our discussion is based on the relative permeability data.

The data from Table 1 shows that the *WR* was in range of 61.6-69.38% while the K_{rCO2} was in range of 0.11.2-0.203. The data show that increasing fluid pressure and injection rate caused an increase in the *WR*; the highest increase occurred with increasing injection rate. On the other hand, the increase in the experimental temperature and water salinity caused a decrease in the *WR*; the highest reduction occurred as brine concentration and valency increased. The *WR* increased by around 2% as the fluid pressure increased from 60 to 70 bar at 0.4 ml/min and by about 0.7% as the pressure increased from 60 to 70 bar at 1 ml/min. The *WR* increased by around 3.5% as the injection rate increased from 0.4 to 1 ml/min at 60 bar. Nevertheless, the *WR* decreased by around 0.8% as the temperature increased from 20 to 29 °C at 90 bar. The *WR* decreased by about 2.7, 5.3, and 6.3 when 1% NaCl, 5% NaCl, and 1% $CaCl_2$ solutions were used instead of deionised water, respectively. The efficiency of water displacement depends on many factors such as permeability, displacement pattern, injection rate, stability of the displacement front, *Ca*, and *M* [22, 54]. The increase in injection rate can enhance production by changing the displacement pattern from capillary to viscous fingering, stabilizing the displacement front, and forcing the injected CO_2 to displace water from low permeability formations [22]. However, the most influential dimensionless parameters that determine the displacement efficiency of CO_2-water core flooding are the *Ca* and *M* [1]. The data from Table 1 reveal that the increase in the *WR* with the increasing fluid pressure and injection rate and the reduction in the *WR* with the increasing temperature can be associated with the change in *Ca* and *M* data. However, the *Ca* data are not available for the set of data dealing with the salinity impact as contact angle data are not available. Nevertheless, the reduction in water recovery with increasing the salinity can be attributed to the increase in capillary forces due to increasing CO_2-brine interfacial tension [86].

On the other hand, the increase in fluid pressure, experimental temperature, injection rate and salinity led to a reduction in the K_{rCO2}. The highest reduction in the K_{rCO2} occurred with increasing temperature whiles the lowest

occurred with increasing pressure. As the CO_2 injection rate increased, the percentage of the reduction in the K_{rCO2} with fluid pressure decreased; this can be related to increasing viscous forces and decreasing viscous forces which leads to reducing the entrapment impact of capillary forces. The K_{rCO2} decreased by around 0.008 as the pressure increased from 60 to 70 bar at 0.4 ml/min and decreased by about 0.002 as the pressure increased from 60 to 70 bar at 1 ml/min. It decreased by around 0.091 as the temperature increased from 20 to 29 °C at 90 bar. It decreased by around 0.056 as the injection rate increased from 0.4 to 1 ml/min at 60 bar. It decreased by about 0.004, and 0.014 when 5% NaCl, and 1% $CaCl_2$ solutions were used instead of deionised water, respectively. However, using 1% NaCl instead of deionised water showed a slight increase in the K_{rCO2}, it increased by about 0.008. The reduction in the K_{rCO2} with increasing temperature and salinity might be related to the increase in the capillary forces and hence reducing the sweeping efficiency. However, this cannot explain the reduction in the K_{rCO2} with increasing pressure and injection rate, the reason for this reduction is not clear. The reduction in the K_{rCO2} with increasing salinity agrees with the findings of Rathnaweera et al. [40].

Table 1: Effect of fluid pressure, temperature, salinity, and injection rate on the endpoint CO_2 effective (relative) permeability and water recovery.

Parameter	*Experiment*	*K_{fCO2} (md)*	*K_{rCO2}*	*WR*	*M*	*Ca*
Pressure Effect	LCO_2-DIW-60 bar-0.4 ml-20 °C	3.188	0.203	65.9	14.33	2.175E-07
	LCO_2-DIW-70 bar-0.4 ml-20 °C	3.064	0.195	67.87	13.4	2.734E-07
	LCO_2-DIW-60 bar-1 ml-20 °C	2.307	0.147	69.38	14.33	5.437E-07
	LCO_2-DIW-70 bar-1 ml-20 °C	2.271	0.145	70.1	13.4	6.835E-07
Temperatur-e Effect	LCO_2-DIW-90 bar-0.1 ml-20 °C	3.185	0.203	65.3	12.24	6.923E-08
	LCO_2-DIW-90 bar-0.1 ml-29 °C	1.760	0.112	66.1	12.73	6.124E-08
Injection Rate Effect	LCO_2-DIW-60 bar-0.4 ml-20 °C	3.188	0.203	65.9	14.33	2.175E-07
	LCO_2-DIW-60 bar-1 ml-20 °C	2.307	0.147	69.38	14.33	5.437E-07
Salinity Effect	LCO_2-DIW-70 bar-0.4 ml-20 °C	3.248	0.195	67.87	13.4	
	LCO_2-1% NaCl-70 bar-0.4 ml-20 °C	3.180	0.203	65.14	13.4	
	LCO_2-5% NaCl-70 bar-0.4 ml-20 °C	2.991	0.191	62.54	13.4	
	LCO_2-1% $CaCl_2$-70 bar-0.4 ml-20 °C	2.845	0.181	61.6	13.4	

4 Conclusion

In this paper, the effect of fluid pressure, temperature, injection rate, and salinity (brine concentration and valency) on the two-phase flow characteristics when liquid CO_2 is injected into a water or brine-saturated sandstone core sample have been investigated in detail. The results indicate that capillary forces have less impact on the differential pressure profiles than viscous forces when fluid pressure, temperature and injection rate increase but the capillary forces have more impact when salinity increase.

The differential pressure profile can be characterized by: (**a**) no change in its shape with increasing pressure, (**b**) oscillations and an increase in the differential pressure profile at the end of the displacements with increasing temperature, (**c**) a spike in the differential pressure profile after the initial increase with increasing injection rate, and (**d**) only a slight change, mainly during the first period, with increasing salinity. The profile of the differential pressure profile can be used an indicator for the period of only water production (quasi-stable pressure reduction), mixed production (high-pressure production), and only CO_2 production (gradual pressure reduction). The appearance of oscillations might reflect the increase in capillary forces impact with increasing temperature; these oscillations can result

in an increase in the residual CO_2 saturation due to the accompanied occurrence of a re-imbibition process of the wetting phase.

The order of the differential pressure with increasing salinity was as follows: LCO_2-1% $CaCl_2$ > LCO_2-5% NaCl > LCO_2-1% NaCl > LCO_2-DIW. The increase in differential pressure with fluid pressure and injection rate and the reduction in it with increasing temperature indicate that viscous forces are more influential than capillary forces at a high injection flowrate. Increasing the differential pressure with the slight increase in salinity indicates that capillary forces dominate the multi-phase flow as no practical change in viscous forces are expected with this slight addition of salts to water. Since capillary forces have a direct impact on the entry pressure and capillary number, then as capillary forces reduces with increasing pressure, temperature, and injection rate, it is expected to result in an easy upward migration of CO_2, thereby affecting the storage capacity and integrity of the sequestered CO_2, as well as result in increasing displacement efficiency. However, as capillary forces impact increase with salinity, it is anticipated to result in a more secure storage of CO_2 and reducing the displacement efficiency. In summary, in order to decide the extent of change in storage capacity and security of a CO_2 project with the change in the above investigated parameters, qualitative studies are required to determine the size of change in both capillary forces and buoyancy forces.

The cumulative produced volumes: (a) decreased slightly with increasing fluid pressure and salinity, and (b) showed no noticeable change with increasing temperature and injection rate. The amounts of injected CO_2 volumes to achieve the highest water recovery (*WR)* were reduced as injection rate increased.

The *WR* was in range of 61.6-69.38% while relative permeability was in range of 0.112-0.203. The results reveal that increasing fluid pressure and injection rate caused an increase in the *WR*. The increase in the experimental temperature and water salinity caused a decrease in the *WR*.. The increase in fluid pressure, experimental temperature, injection rate and salinity led to a reduction in the endpoint CO_2 relative permeability. As the CO_2 injection rate increased, the percentage of the reduction in the endpoint CO_2 relative permeability decreased with increasing fluid pressure.

Acknowledgements: The authors wish to thank the Higher Committee for Education Development in Iraq and the Ministry of Oil in Iraq for their sponsorship of the first author PhD study.

5 References

1. Kazemifar F, Blois G, Kyritsis DC, Christensen KT. Quantifying the flow dynamics of supercritical CO2–water displacement in a 2D porous micromodel using fluorescent microscopy and microscopic PIV. Advances in Water Resources. 2015.
2. Hangx S, van der Linden A, Marcelis F, Bauer A. The effect of CO2 on the mechanical properties of the captain sandstone: geological storage of CO2 at the Goldeneye field (UK). International Journal of Greenhouse Gas Control. 2013;19:609-19.
3. Bachu S. Geological sequestration of anthropogenic carbon dioxide: applicability and current issues. Geological perspectives of global climate change. 2001(47):285-303.
4. Tutolo BM, Luhmann AJ, Kong X-Z, Saar MO, Seyfried WE. CO2 sequestration in feldspar-rich sandstone: coupled evolution of fluid chemistry, mineral reaction rates, and hydrogeochemical properties. Geochimica et Cosmochimica Acta. 2015;160:132-54.
5. Kaveh NS, Wolf K, Ashrafizadeh S, Rudolph E. Effect of coal petrology and pressure on wetting properties of wet coal for CO2 and flue gas storage. International Journal of Greenhouse Gas Control. 2012;11:S91-S101.
6. Delshad M, Wheeler MF, Kong X, editors. A critical assessment of CO2 injection strategies in saline aquifers. SPE Western Regional Meeting; 2010: Society of Petroleum Engineers.
7. Gozalpour F, Ren S, Tohidi B. CO2 EOR and storage in oil reservoir. Oil & gas science and technology. 2005;60(3):537-46.
8. Plug W-J, Bruining J. Capillary pressure for the sand–CO2–water system under various pressure conditions. Application to CO2 sequestration. Advances in Water Resources. 2007;30(11):2339-53.
9. Teng H, Yamasaki A. Mass transfer of CO2 through liquid CO2–water interface. International journal of heat and mass transfer. 1998;41(24):4315-25.
10. Sohrabi M, Jamiolahmady M, Al Quraini A, editors. Heavy Oil Recovery by Liquid CO2/Water Injection. EUROPEC/EAGE Conference and Exhibition; 2007; London, UK 11–14 June 2007: Society of Petroleum Engineers: Houston, TX, USA, 2007.
11. Nourpour Aghbash V, Ahmadi M, editors. Evaluation of CO2-EOR and Sequestration in Alaska West Sak Reservoir Using Four-Phase Simulation Model. SPE Western Regional Meeting; 2012; Bakersfield, CA, USA, 21–23 March 2012: Society of Petroleum Engineers: Houston, TX, USA, 2012.

12. Espinoza DN, Santamarina JC. Water-CO2-mineral systems: Interfacial tension, contact angle, and diffusion—Implications to CO2 geological storage. Water resources research. 2010;46(7).
13. Bachu S. Sequestration of CO2 in geological media: criteria and approach for site selection in response to climate change. Energy conversion and management. 2000;41(9):953-70.
14. Saraji S, Piri M, Goual L. The effects of SO2 contamination, brine salinity, pressure, and temperature on dynamic contact angles and interfacial tension of supercritical CO2/brine/quartz systems. International Journal of Greenhouse Gas Control. 2014;28:147-55.
15. Frailey SM, Grube JP, Seyler B, Finley RJ, editors. Investigation of liquid CO2 sequestration and EOR in low temperature oil reservoirs in the Illinois basin. SPE/DOE Symposium on Improved Oil Recovery; 2004; Tulsa, OK, USA, 17–21 April 2004: Society of Petroleum Engineers: Houston, TX, USA, 2004.
16. Hamdi Z, Awang M. Comparison of Liquid CO2 Injection with a Common Tertiary Recovery Method Using Non-Isothermal Simulations. ICIPEG 2016: Springer; 2017. p. 61-70.
17. Basbug B, Gumrah F, Oz B, editors. Simulating the Effects of Deep Saline Aquifer Properties on CO2 Sequestration. Canadian International Petroleum Conference; 2005: Petroleum Society of Canada.
18. Herring AL, Andersson L, Newell D, Carey J, Wildenschild D. Pore-scale observations of supercritical CO2 drainage in Bentheimer sandstone by synchrotron x-ray imaging. International Journal of Greenhouse Gas Control. 2014;25:93-101.
19. Kaveh NS, Rudolph ESJ, van Hemert P, Rossen WR, Wolf KH. Wettability Evaluation of a CO2/Water/Bentheimer Sandstone System: Contact Angle, Dissolution, and Bubble Size. Energy & Fuels. 2014;28(6):4002-20.
20. Kaveh NS, Rossen W, Rudolph-Floter SEJ, Berentsen C, editors. Wettability Determination by Equilibrium Contact Angle Measurements Reservoir Rock-Connate Water System with Injection of CO2 (SPE 154382). 74th EAGE Conference and Exhibition incorporating EUROPEC 2012; 2012.
21. Pentland C, El-Maghraby R, Georgiadis A, Iglauer S, Blunt M. Immiscible displacements and capillary trapping in CO2 storage. Energy Procedia. 2011;4:4969-76.
22. Zhang C, Oostrom M, Grate JW, Wietsma TW, Warner MG. Liquid CO2 Displacement of Water in a Dual-Permeability Pore Network Micromodel. Environmental science & technology. 2011;45(17):7581-8.
23. Saraji S, Goual L, Piri M, Plancher H. Wettability of supercritical carbon dioxide/water/quartz systems: simultaneous measurement of contact angle and interfacial tension at reservoir conditions. Langmuir : the ACS journal of surfaces and colloids. 2013;29(23):6856-66.
24. Wang D, Dong B, Breen S, Zhao M, Qiao J, Liu Y, et al. Review: Approaches to research on CO2/brine two-phase migration in saline aquifers. Hydrogeology Journal. 2015;23(1):1-18.
25. Levine JS, Matter JM, Goldberg DS, Lackner KS, Supp MG, Ramakrishnan T. Two phase brine-CO2 flow experiments in synthetic and natural media. Energy Procedia. 2011;4:4347-53.
26. Qi R, Laforce T, Blunt M. Carbon Dioxide (CO2) Injection Design to Maximize Underground Reservoir Storage and Enhanced Oil Recovery (EOR). Developments and Innovation in Carbon Dioxide (CO2) Capture and Storage Technology (Ed MM Maroto-Valer), Woodhead Publishing Series in Energy, Oxford. 2010:169-84.
27. Arif M, Jones F, Barifcani A, Iglauer S. Electrochemical investigation of the effect of temperature, salinity and salt type on brine/mineral interfacial properties. International Journal of Greenhouse Gas Control. 2017;59:136-47.
28. Wu S, Firoozabadi A. Effect of salinity on wettability alteration to intermediate gas-wetting. SPE Reservoir Evaluation & Engineering. 2010;13(02):228-45.
29. Yang D, Gu Y, Tontiwachwuthikul P. Wettability determination of the reservoir brine− reservoir rock system with dissolution of CO2 at high pressures and elevated temperatures. Energy & Fuels. 2007;22(1):504-9.
30. Liu N, Ghorpade SV, Harris L, Li L, Grigg RB, Lee RL, editors. The effect of pressure and temperature on brine-CO2 relative permeability and IFT at reservoir conditions. In Proceedings of theSPE Eastern Regional Meeting; 2010; Morgantown, WV, USA, 13–15 October 2010: Society of Petroleum Engineers: Houston, TX, USA, 2010.
31. Al-Aulaqi T, Fisher Q, Grattoni C, Al-Hinai SM, editors. Wettability Alteration by Brine Salinity and Temperature in Reservoir Cores. SPE Saudi Arabia Section Technical Symposium and Exhibition; 2013: Society of Petroleum Engineers.
32. Bachu S, Bennion DB. Interfacial tension between CO2, freshwater, and brine in the range of pressure from (2 to 27) MPa, temperature from (20 to 125)° C, and water salinity from (0 to 334 000) mg· L− 1. Journal of Chemical & Engineering Data. 2008;54(3):765-75.
33. Krevor S, Reynolds C, Al-Menhali A, Niu B. The Impact of Reservoir Conditions and Rock Heterogeneity on CO2-Brine Multiphase Flow in Permeable Sandstone. Petrophysics. 2016;57(01):12-8.

34. Alkan H, Cinar Y, Ülker E. Impact of capillary pressure, salinity and in situ conditions on CO2 injection into saline aquifers. Transport in porous media. 2010;84(3):799-819.
35. Al-Menhali A, Krevor S. Effective wettability measurements of CO2-brine-sandstone system at different reservoir conditions. Energy Procedia. 2014;63:5420-6.
36. Cutts RE. Experimental investigation of the influence of surface energy and pore fluid characteristics on the behavior of partially saturated coarse-grained soils. 2009.
37. Leelamanie D, Karube J. Soil-water contact angle as affected by the aqueous electrolyte concentration. Soil Science and Plant Nutrition. 2013;59(4):501-8.
38. Alotaibi MB, Nasralla RA, Nasr-El-Din HA. Wettability studies using low-salinity water in sandstone reservoirs. SPE Reservoir Evaluation & Engineering. 2011;14(06):713-25.
39. Nasralla RA, Bataweel MA, Nasr-El-Din HA, editors. Investigation of Wettability Alteration by Low Salinity Water in Sandstone Rock. Offshore Europe; 2011: Society of Petroleum Engineers.
40. Rathnaweera T, Ranjith P, Perera M. Effect of salinity on effective CO2 permeability in reservoir rock determined by pressure transient methods: An experimental study on Hawkesbury sandstone. Rock Mechanics and Rock Engineering. 2015;48(5):2093-110.
41. Sharma G, Mohanty K. Wettability alteration in high-temperature and high-salinity carbonate reservoirs. SPE Journal. 2013;18(04):646-55.
42. Shehata AM, Alotaibi MB, Nasr-El-Din HA. Waterflooding in carbonate reservoirs: Does the salinity matter? SPE Reservoir Evaluation & Engineering. 2014;17(03):304-13.
43. Zhang Y, Xie X, Morrow NR, editors. Waterflood performance by injection of brine with different salinity for reservoir cores. SPE Annual Technical Conference and Exhibition; 2007: Society of Petroleum Engineers.
44. Dang CT, Nghiem LX, Chen Z, Nguyen QP, Nguyen NT, editors. State-of-the art low salinity waterflooding for enhanced oil recovery. SPE Asia Pacific Oil and Gas Conference and Exhibition; 2013: Society of Petroleum Engineers.
45. Al-Yaseri AZ, Lebedev M, Barifcani A, Iglauer S. Receding and advancing (CO2+ brine+ quartz) contact angles as a function of pressure, temperature, surface roughness, salt type and salinity. The Journal of Chemical Thermodynamics. 2015.
46. Alshakhs MJ, Kovscek AR. Understanding the role of brine ionic composition on oil recovery by assessment of wettability from colloidal forces. Advances in colloid and interface science. 2015.
47. Tang G, Morrow NR. Salinity, temperature, oil composition, and oil recovery by waterflooding. SPE Reservoir Engineering. 1997;12(04):269-76.
48. Xu W, Ayirala SC, Rao DN. Compositional Dependence of Wetting and Contact Angles in Solid-Liquid-Liquid Systems under Realistic Environments. The Canadian Journal of Chemical Engineering. 2006;84(1):44-51.
49. Cao SC, Dai S, Jung J. Supercritical CO2 and brine displacement in geological carbon sequestration: Micromodel and pore network simulation studies. International Journal of Greenhouse Gas Control. 2016;44:104-14.
50. Jobard E, Sterpenich J, Pironon J, Corvisier J, Jouanny M, Randi A. Experimental simulation of the impact of a thermal gradient during geological sequestration of CO2: The COTAGES experiment. International Journal of Greenhouse Gas Control. 2013;12:56-71.
51. Ma J, Petrilli D, Manceau J-C, Xu R, Audigane P, Shu L, et al. Core scale modelling of CO2 flowing: identifying key parameters and experiment fitting. Energy Procedia. 2013;37:5464-72.
52. Xu R, Luo S, Jiang P. Pore scale numerical simulation of supercritical CO2 injecting into porous media containing water. Energy Procedia. 2011;4:4418-24.
53. Berg S, Oedai S, Ott H. Displacement and mass transfer between saturated and unsaturated CO2–brine systems in sandstone. International Journal of Greenhouse Gas Control. 2013;12:478-92.
54. Song Y, Jiang L, Liu Y, Yang M, Zhao Y, Zhu N, et al. An experimental study on CO2/water displacement in porous media using high-resolution magnetic resonance imaging. International Journal of Greenhouse Gas Control. 2012;10:501-9.
55. Suekane T, Soukawa S, Iwatani S, Tsushima S, Hirai S. Behavior of supercritical CO2 injected into porous media containing water. Energy. 2005;30(11):2370-82.
56. Chang C, Zhou Q, Xia L, Li X, Yu Q. Dynamic displacement and non-equilibrium dissolution of supercritical CO2 in low-permeability sandstone: An experimental study. International Journal of Greenhouse Gas Control. 2013;14:1-14.
57. Suenaga H, Nakagawa K. Analysis of two-phase flow properties of sandstones to evaluate their suitability for geologic storage of CO2. Energy Procedia. 2011;4:4323-30.

58. Krevor S, Pini R, Benson SM. Measurement of the multiphase flow properties of the CO2 brine system for carbon sequestration. Energy Procedia. 2013;37:4499-503.
59. Wang D, Zhao M, Song Y, Xu H, Ma X. Influence of Capillary Pressure and Injection Rate as well as Heterogeneous and Anisotropic Permeability on CO2 Transport and Displacement Efficiency in Water-Saturated Porous Media. Energy Procedia. 2013;37:3945-51.
60. Alemu BL, Aker E, Soldal M, Johnsen Ø, Aagaard P. Influence of CO2 on rock physics properties in typical reservoir rock: a CO2 flooding experiment of brine saturated sandstone in a CT-scanner. Energy Procedia. 2011;4:4379-86.
61. Saeedi A, Rezaee R, Evans B, Clennell B. Multiphase flow behaviour during CO2 geo-sequestration: Emphasis on the effect of cyclic CO2–brine flooding. Journal of Petroleum Science and Engineering. 2011;79(3):65-85.
62. Perrin J-C, Benson S. An experimental study on the influence of sub-core scale heterogeneities on CO2 distribution in reservoir rocks. Transport in porous media. 2010;82(1):93-109.
63. Shi J-Q, Xue Z, Durucan S. Supercritical CO2 core flooding and imbibition in Tako sandstone—Influence of sub-core scale heterogeneity. International Journal of Greenhouse Gas Control. 2011;5(1):75-87.
64. Ott H, Pentland C, Oedai S. CO2–brine displacement in heterogeneous carbonates. International Journal of Greenhouse Gas Control. 2015;33:135-44.
65. Ott H, de Kloe K, Marcelis F, Makurat A. Injection of supercritical CO2 in brine saturated sandstone: pattern formation during salt precipitation. Energy Procedia. 2011;4:4425-32.
66. Islam A, Chevalier S, Sassi M. Experimental and Numerical Studies of CO2 Injection Into Water-Saturated Porous Medium: Capillary to Viscous to Fracture Fingering Phenomenon. Energy Procedia. 2013;37:5511-9.
67. Jiang L, Yu M, Liu Y, Yang M, Zhang Y, Xue Z, et al. Behavior of CO2/water flow in porous media for CO2 geological storage. Magnetic Resonance Imaging. 2017;37:100-6.
68. Yu M, Song Y, Jiang L, Li W. CO2/Water Displacement in Porous Medium Under Pressure and Temperature Conditions for Geological Storage. Energy Procedia. 2014;61:282-5.
69. Manceau J-C, Ma J, Li R, Audigane P, Jiang P, Xu R, et al. Two-phase flow properties of a sandstone rock for the CO2/water system: Core-flooding experiments, and focus on impacts of mineralogical changes. Water Resources Research. 2015;51(4):2885-900.
70. Rezaei N, Firoozabadi A. Pressure evolution and production performance of waterflooding in n-heptane-saturated fired berea cores. SPE Journal. 2014;19(04):674-86.
71. Al-Zaidi E, Nash J, Fan X. Effect of CO2 phase on its water displacements in a sandstone core sample. International Journal of Greenhouse Gas Control. 2018;71:227-38.
72. Al-Zaidi E, Fan X. Effect of aqueous electrolyte concentration and valency on contact angle on flat glass surfaces and inside capillary glass tubes. Colloids and Surfaces A: Physicochemical and Engineering Aspects. 2018;543:1-8.
73. Al-Zaidi E, Fan X, Edlmann K. The Effect of CO2 Phase on Oil Displacement in a Sandstone Core Sample. Fluids. 2018;3(1):23.
74. Bikkina P, Wan J, Kim Y, Kneafsey TJ, Tokunaga TK. Influence of wettability and permeability heterogeneity on miscible CO2 flooding efficiency. Fuel. 2016;166:219-26.
75. Chatzis I, Morrow NR. Correlation of capillary number relationships for sandstone. Society of Petroleum Engineers Journal. 1984;24(05):555-62.
76. Fulcher Jr RA, Ertekin T, Stahl C. Effect of capillary number and its constituents on two-phase relative permeability curves. Journal of Petroleum Technology. 1985;37(02):249-60.
77. Schembre JM, Kovscek AR. A technique for measuring two-phase relative permeability in porous media via X-ray CT measurements. Journal of Petroleum Science and Engineering. 2003;39(1-2):159-74.
78. Akbarabadi M, Piri M. Relative permeability hysteresis and capillary trapping characteristics of supercritical CO2/brine systems: An experimental study at reservoir conditions. Advances in Water Resources. 2013;52:190-206.
79. Chiquet P, Broseta DF, Thibeau S, editors. Capillary alteration of shaly caprocks by carbon dioxide. In Proceedings of the SPE Europec/EAGE Annual Conference; 2005; Madrid, Spain, 13–16 June 2005: Society of Petroleum Engineers: Houston, TX, USA, 2005.
80. Chiquet P, Daridon J-L, Broseta D, Thibeau S. CO2/water interfacial tensions under pressure and temperature conditions of CO2 geological storage. Energy Conversion and Management. 2007;48(3):736-44.
81. Farokhpoor R, Bjørkvik BJA, Lindeberg E, Torsæter O. Wettability behaviour of CO2 at storage conditions. International Journal of Greenhouse Gas Control. 2013;12:18-25.

675 82. Han F, Busch A, van Wageningen N, Yang J, Liu Z, Krooss BM. Experimental study of gas and water
676 transport processes in the inter-cleat (matrix) system of coal: anthracite from Qinshui Basin, China. International
677 Journal of Coal Geology. 2010;81(2):128-38.
678 83. Li X. Experimental Studies on Pore Wetting and Displacement of Fluid by CO2 in Porous Media [doctoral
679 thesis]: University of Edinburgh, Edinburgh, UK; 2015.
680 84. Nutt C, editor The physical basis of the displacement of oil from porous media by other fluids: a capillary
681 bundle model. Proceedings of the Royal Society of London A: Mathematical, Physical and Engineering Sciences; 1982:
682 The Royal Society.
683 85. Kwelle SO. Experimental studies on resistance to fluid displacement in single pores [Ph.D. Thesis]: The
684 University of Edinburgh, Edinburgh, UK; 2017.
685 86. Chalbaud C, Robin M, Lombard JM, Martin F, Egermann P, Bertin H. Interfacial tension measurements and
686 wettability evaluation for geological CO2 storage. Advances in Water Resources. 2009;32(1):98-109.
687 87. Bennion DB, Bachu S, editors. The impact of interfacial tension and pore size distribution/capillary pressure
688 character on CO2 relative permeability at reservoir conditions in CO2-brine systems. In Proceedings of the SPE/DOE
689 Symposium on Improved Oil Recovery; 2006; Tulsa, OK, USA, 22–26 April 2006: Society of Petroleum Engineers:
690 Houston, TX, USA, 2006.
691 88. Tokunaga TK, Wan J. Capillary Pressure and Mineral Wettability Influences on Reservoir CO2 Capacity.
692 Reviews in Mineralogy and Geochemistry. 2013;77(1):481-503.
693 89. Ji X, Zhu C. CO2 storage in deep saline aquifers. Chapter 10 in Novel Materials for Carbon Dioxide Mitigation
694 Technology. 2015:299-332.
695 90. De Silva G, Ranjith P, Perera M. Geochemical aspects of CO2 sequestration in deep saline aquifers: A review.
696 Fuel. 2015;155:128-43.
697 91. Busch A, Müller N. Determining CO2/brine relative permeability and capillary threshold pressures for
698 reservoir rocks and caprocks: Recommendations for development of standard laboratory protocols. Energy Procedia.
699 2011;4:6053-60.
700 92. Akbarabadi M, Piri M. Geologic storage of carbon dioxide: an experimental study of permanent capillary
701 trapping and relative permeability. In Proceedings of International Symposium of the Society of Core Analysts;
702 Austin, Texas, USA. 18–21 September 20112011. p. 18-21.
703 93. Peace software. 2017 [Available from: http://www.peacesoftware.de/einigewerte/co2_e.html.